

Cite this: *Digital Discovery*, 2026, 5, 1689

# Siamese graph neural networks for melting temperature prediction of molten salt eutectics

Nila Mandal, James Maniscalco, Mark Aindow and Qian Yang\*

High-throughput screening enabled by structure–property prediction models is a powerful approach for accelerating materials discovery. However, while machine learning of structure–property models have become widespread, its application to mixtures remains limited due to increased complexity and the scarcity of available data. Machine learning methods for high-throughput screening of eutectic mixtures have been proposed in recent years, but there remain challenges due to the lack of diverse, open-access datasets and the need for feature engineering based on chemical knowledge. To overcome these limitations, we propose a method using Siamese graph neural networks trained solely on structural information, without requiring any prior chemical descriptors, to predict eutectic melting temperatures. We demonstrate on a dataset of molten salt eutectics that this approach can reach similar performance to chemistry-based models that require significantly more prior knowledge. We show that lower-order mixtures may be used to augment data on higher-order mixtures. Interestingly, our model trained on inorganic molten salts seems to learn information about the ideal mixture model. We also evaluate the efficacy of using our inorganic molten salt model for transfer learning with a variety of organic eutectic mixtures.

Received 28th October 2025

Accepted 1st March 2026

DOI: 10.1039/d5dd00480b

rsc.li/digitaldiscovery

## 1 Introduction

Mixture properties, such as eutectic melting temperatures, are critical for materials design. For example, molten salt eutectic mixtures have the potential to be highly effective in several sustainable energy applications. They have gained attention in recent years in research on battery electrolytes,<sup>1</sup> solar power,<sup>2</sup> thermal energy storage materials,<sup>2</sup> and nuclear reactors.<sup>3</sup>

These important applications are hindered by drawbacks of existing computational and experimental methods for determining mixture properties, which are often slow and resource-intensive. A machine learning approach for high-throughput screening of eutectic melting temperatures is thus highly desirable. However, such approaches are often hindered by the lack of diverse, publicly available experimental datasets and the computational cost of simulation methods for generating data. As a result, most recent studies rely on classical machine learning algorithms with highly informative but expensive engineered features that can be effectively trained on smaller datasets. In this work, we demonstrate that a deep learning-based approach leveraging only structural information is sufficient to train effective models for predicting eutectic melting temperatures of binary molten salt mixtures, using a dataset of 2244 data points. Our approach utilizes Siamese graph neural networks<sup>4</sup> and incorporates ideas from Janossy pooling<sup>5</sup> to effectively handle mixtures. We also demonstrate that

individual components' melting point data can be used to augment the mixture datasets, and produce models that can extrapolate from inorganic to organic materials (Fig. 1).

Our architecture includes several novel contributions, including the ability to learn melting points of binary eutectic mixtures from structural data alone, and the ability to learn a model correlated with the ideal thermodynamic model without requiring single component melting points or enthalpy values, or eutectic compositions  $x_e$  values. Although single component melting points are not required, we also demonstrate that by optionally using them as additional datapoints for data augmentation rather than features, we can further improve our model's predictive performance as well as achieve good predictions for previously unknown single component melting temperatures.

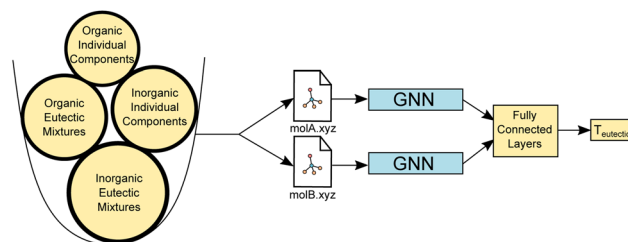


Fig. 1 Using only structural information, our architecture can produce permutation-invariant predictions for eutectic melting temperatures. The molecule embedding learned by the GNN from inorganic structures can also be used for transfer learning to organic structures.

University of Connecticut, Storrs, CT, USA. E-mail: qyang@uconn.edu



## 2 Background

### 2.1 Melting point prediction

A material's melting point is an important property to consider for any application requiring a solvent or electrolyte, and melting point prediction has long been a goal of computational chemistry. Molecular dynamics simulations can be used to estimate materials' melting points; however, simulations of a solid material melting tend to result in overestimates of melting point, while simulations of a liquid material solidifying tend to underestimate the melting point. In addition, defects can cause materials to melt at lower temperatures than would be expected of a perfect material as represented in a simulation.<sup>6</sup>

Much work has been done on melting point prediction for ionic liquids, including comparisons of methods such as k-nearest neighbor regression, gradient boosting, random forests, support vector machines, and graph neural networks.<sup>7,8</sup> Structural descriptors such as molecule fingerprints, Coulomb matrices, or other engineered features can be used to improve prediction accuracy. Fingerprints which encode functional groups have been found to be particularly effective.<sup>9</sup> However, Acar *et al.*<sup>10</sup> argues that all of these fingerprint methods are expensive to compute, and not practical for either large datasets or datasets which include large molecules. Instead, they test a very simple fully connected neural network with one dropout layer, and compare the correlation between melting point and the various engineered features they use. Although these engineered features may be less computationally complex than the fingerprint methods evaluated by Low *et al.*,<sup>9</sup> expertise in chemistry is necessary in order to understand and generate these descriptors for any dataset.

### 2.2 Eutectic materials

Eutectic mixtures are mixtures which have a lower melting point than either of its individual mixture components; as such, they

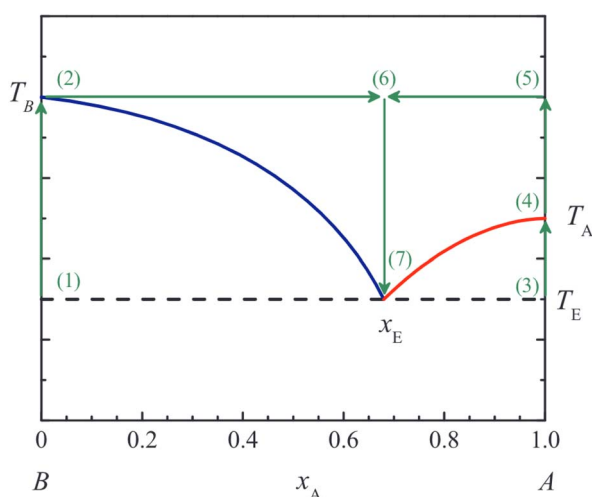


Fig. 2 From ref. 11, a phase diagram illustrating the relationships between  $T_a$ ,  $T_b$ ,  $x_e$ , and  $T_e$ . Eutectic mixtures are mixtures with a melting point lower than that of the individual components of the mixture. The mixture proportion with the lowest possible melting temperature is referred to as  $x_e$ , and that melting temperature is referred to as  $T_e$ .<sup>†1</sup>

are often desirable for applications that require low-melting point materials. In our work we focus on binary eutectics. We refer to a mixture's minimum eutectic melting point as  $T_e$ , and refer to the mixture ratio as  $x_e$  (Fig. 2).

Determining eutectic melting points is challenging for materials screening because it is infeasible to manually test every possible mixture of candidate components. Research into data-driven approaches to  $T_e$  prediction has been significantly hindered by the lack of large, publicly available datasets. Although published eutectic datasets exist, they are often small (100 examples or less) and focused on a highly specific family of materials (for example, fatty acids or organic explosives). Due to these limited dataset sizes, machine learning approaches to eutectic melting point prediction typically rely on highly informative chemical descriptors such as individual melting points, enthalpies of melting, and  $x_e$  values, which are themselves difficult to obtain or compute.

If all of those values are available,  $T_e$  can be computed using the ideal thermodynamic model (ITM). However, if any of these values are unavailable in existing literature for a given material, it is impossible for the ITM to compute  $T_e$  for any mixture which includes that material. Even when all necessary values are known, the predicted  $T_e$  values from the ITM are not perfect. For example, Ravichandran *et al.*<sup>1</sup> found that for their data, the ITM predictions had a root mean squared error (RMSE) of 86.6 K. The correlation between  $T_e$  and the individual melting points of the mixture components has been used to estimate how much melting point depression the eutectic mixture will have;<sup>12</sup> however, even this extremely rough estimation requires knowledge of the melting points of each individual component, which is itself challenging to obtain for new materials exploration.

Ravichandran *et al.*<sup>1</sup> approach eutectic  $T_e$  prediction for molten salts by using an ensemble model composed of the ideal thermodynamic model, a gradient boosting model, and a Roost model. Of these, the Roost model is the only part of the ensemble which does not require expensive engineered features. The ensemble model, referred to in the text as the "mean model," takes the average of the three models' predictions to determine its final output. They consider mixtures of up to six eutectic components, and their data is a subset of the experimentally-determined molten salt eutectic mixtures, proportions, and  $T_e$  values compiled by Janz *et al.*<sup>13</sup> Our work considers a different subset of mixtures from the same compilation.

There are several smaller datasets we are aware of for different families of organic eutectic mixtures. Kahwaji *et al.*<sup>11</sup> published a set of fatty acid eutectics as well as a computational method that they designed to support eutectic phase change materials exploration. Guendouzi *et al.*<sup>14</sup> published a set of melting points for individual fatty acids, which overlap with Kahwaji's individual components. Luu *et al.*<sup>15</sup> and Lavrinenko *et al.*<sup>16</sup> both published sets of deep eutectic solvents drawn from literature, with substantial overlap between the mixtures they compiled. More recently, databases for binary and ternary DES and corresponding ML models have also been developed.<sup>17</sup>



### 2.3 Graph neural networks

Graph neural networks provide a compelling approach to structure–property prediction because they can learn directly from structural data without the need for complex engineered features. As such, they have become a popular way to learn structure–property relationships for molecules and materials. A graph neural network (GNN) takes as input one or more graphs, which are made up of nodes and edges, and can solve problems either at the node level or the graph level. For example, predicting the melting point of a single component molecule from its graph structure is a graph-level problem. Most GNNs follow the message-passing framework,<sup>18</sup> in which each layer of the neural network computes a function of each node and its one-hop neighbor's features, including edge features if present. After one layer, each node has aggregated a representation of its entire one-hop neighborhood; after two layers each node has aggregated a representation of its two-hop neighborhood, and so on.<sup>19</sup>

AttentiveFP,<sup>20</sup> which is used in this work, is one such message passing graph neural network architecture, with the addition of an attention mechanism to help represent intramolecular interactions beyond each node's one-hop neighborhood. The architecture has a series of layers for atom embedding, followed by a series of layers for molecule embedding. For each graph, AttentiveFP generates a “state node” which is connected to every node in the graph; this is used to aggregate information from the whole graph to compute a learned representation of the entire molecule.

A significant challenge in GNNs is identifying an appropriate pooling method. Graph pooling should generally be order-invariant, because the nodes in a graph typically are not meant to relate to each other in any sequential ordering. However, simple order-invariant methods like mean or max pooling fail to capture important structural information that is not explicitly represented by node features.<sup>21</sup> Learned pooling methods, such as hierarchical pooling or Janossy pooling<sup>5</sup> may produce better pooled representations.

In order to handle mixtures, we incorporate ideas from Janossy pooling,<sup>5</sup> which refers to building permutation-invariant functions by taking the average, or an approximation of the average, of a permutation-sensitive function's output over every possible permutation. In the context of graph neural networks, this refers to permutations of the nodes in the graph. In the general case, an approximation method is necessary for tractability; as such, Murphy *et al.*<sup>5</sup> present three categories of approximation methods. However, in problem domains where the number of possible permutations per input is small, as in this work, it may be reasonable to compute this naively.

### 2.4 Siamese neural networks

In a Siamese neural network, both elements of a pair are passed through a series of identical neural network layers; all weights

are shared between both branches. This means that, at each layer, the weights and biases of the two neural networks are exactly equal. This type of neural network architecture is an intuitive solution to pairwise problems.

Siamese neural networks<sup>4</sup> were originally developed to measure the similarity or difference between pairs of input data. Since determination of binary eutectic  $T_e$  values is an inherently pairwise problem, and  $T_e$  and  $x_e$  are correlated with the difference between the melting points of the mixture components,<sup>12</sup> Siamese neural networks are well-suited to our problem.

Siamese neural networks have been applied to many problems in chemistry and materials science due to their efficacy in one- or few-shot learning and similarity comparison. In particular, they have been widely used to screen molecules for drug discovery, predict molecule solubility or toxicity, and predict drug response similarity.<sup>4,22–24</sup> Siamese graph neural networks have also been used with engineered graph level features for drug-responsiveness prediction on cancer treatments.<sup>25</sup>

## 3 Methods

### 3.1 Graph representation and features

In this work, we develop an order-invariant architecture to predict eutectic mixture  $T_e$  values with minimal input data. First, we generate a graph representation of each molecule, based on structure data drawn from PubChem. Each atom in a molecule is represented as a node in a graph, with node features consisting of the group and period number of the corresponding atom's element. Bonds are represented by edges in the graph; we chose not to include edge features. No additional node- or graph-level features are needed. Our methods do not require any engineered features, and do not require attributes such as individual components melting points or mixture proportions; this means that these methods can be applied to any eutectic data for which the individual components' structures are known (Table 1).

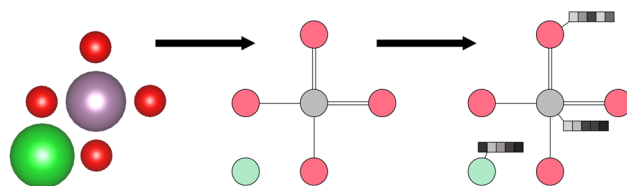


Fig. 3 In a graph representation of a molecule, each node represents an atom and each edge represents a bond. Each node and edge can have a set of features relating to the properties of the associated atom or bond, such as element properties or bond lengths. In our work we use the group and period number of each atom's element as node features and we do not include edge features. In the example above, BaMoO<sub>4</sub>, barium is colored green, molybdenum is gray, and the four oxygen atoms are red. In accordance with the bond definitions drawn from PubChem, the oxygen atoms at the top of the figure shares a double-bond with molybdenum, as does the oxygen atom to the right. Meanwhile, the left and bottom oxygen atoms have single bonds with molybdenum. Because this representation requires only the individual components' structural information, it is possible to use data for which we do not have access to more complex chemical features like individual melting points.

† Reprinted from *Thermochimica Acta*, 660, S. Kahwaji and M. A. White, Prediction of the properties of eutectic fatty acid phase change materials, 94–100, 2018, with permission from Elsevier.



Table 1 We compare our results with several models from other works which require more complex input features

Features required	Our work	ITM <sup>1</sup>	GBM <sup>1</sup>	Roost <sup>1</sup>	CatBoost <sup>17</sup>
Indiv. component melting points		X			X
Indiv. component enthalpy values		X			
Mixture $x_e$				X	X
MAGPIE descriptors <sup>26</sup>			X		
Other engineered features					X
Element composition	X		X	X	X
Molecule graph structure	X				

### 3.2 Inorganic data

We provide a curated dataset of 913 individual molecules paired into 2244 molten salt eutectic pairs and their corresponding experimentally determined melting points. Of those

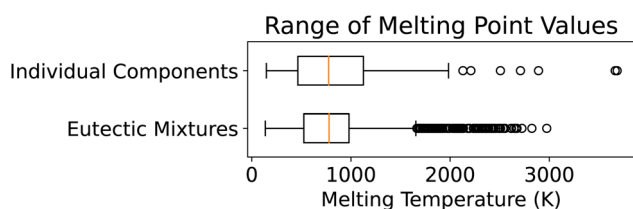


Fig. 4 Box-and-whisker plot of melting temperature range of our data. Our dataset consists of mixtures with  $T_e$  values in the range of 136 to 2975 kelvin, and the distribution of values is skewed towards lower temperatures. One mixture with a  $T_e$  of 4984 K was excluded from experiments. 149 individual components' melting points were found; these were between 147 and 3685 K.

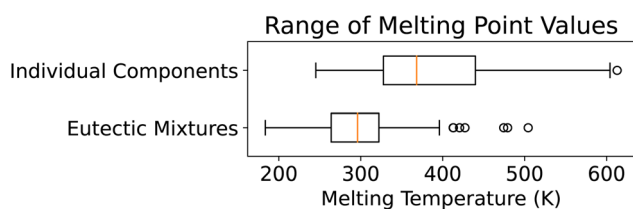


Fig. 5 Melting temperature ranges for DES individual components and mixtures. The vast majority of this dataset is below 500 K, in contrast to our molten salts dataset, which has a much larger temperature range.

individual components, we have individual melting point values for 149 of them. These mixture pairs and  $T_e$  values were drawn from Janz *et al.*,<sup>13</sup> which compiled several thousand experimentally-determined molten salt eutectic mixtures, proportions, and  $T_e$  values from publications prior to 1978. We manually transcribed the molecules listed in this text, and cross-referenced them with PubChem<sup>27</sup> to generate graph representations of each mixture component's solid state structure. The box-and-whisker plot in Fig. 4 depicts the first quartile, median, and third quartile of melting points for the individual components and the mixtures, showing that the dataset is skewed towards lower temperatures. We take a stratified partition of the pairs and individual components to generate a 10-fold cross validation set and a test set.

### 3.3 Organic data

We use a smaller organic dataset comprised of 88 individual components and 239 unique deep eutectic solvent (DES) mixtures drawn from ref. 15–17 for transfer learning experiments to examine our model's ability to extrapolate from inorganic to organic data (Fig. 5). This dataset consisting of both individual component melting temperatures and binary mixture eutectic melting temperatures is partitioned into a 5-fold cross-validation set and a test set for our experiments.

We further use a set of fatty acids,<sup>11</sup> a set of explosives,<sup>12</sup> and a set of quinones<sup>28</sup> which form eutectic mixtures as small test sets for evaluating zero-shot transfer from inorganic to organic eutectics (Table 2).

Table 2 Our work refers to input data on binary eutectic mixtures as A,B data, and refers to input data on individual component melting points as A,A data. We have A,B and A,A training and test sets for both molten salts and deep eutectic solvents. The main works with which we compare our results,<sup>1,17</sup> do not use individual component data for data augmentation. We use the molten salt eutectic data to train our GNN architecture from random initialization. We use the best molten salts model for transfer learning, inputting the DES data and extracting the molecule embedding to train a kernel ridge regression model. The remaining datasets, fatty acids, explosives, and quinones, are used for zero-shot prediction after transfer learning

Dataset	Tasks	Number of data points	Avg. atoms per molecule
Molten salts A,B data	Training from scratch	2244	5
Molten salts A,A data	Training from scratch	149	5
DES A,B data	Transfer learning	239	24
DES A,A data	Transfer learning	88	24
Fatty acids	Inference only	102	43
Explosives	Inference only	74	21
Quinones	Inference only	26	18



### 3.4 Handling noisy duplicates

Several of the mixture pairs in this dataset have duplicate entries with differing values. Some of these are due to the mixture pair forming multiple eutectic points, whereas others are noisy experimental data. Given the advancements in experimental technologies between 1978 and 2023, some of these noisy mixtures may now have more definitive reference values in other literature.

For the purposes of this work, we focus on the minimum  $T_e$  value for each unique mixture pair represented, because we are interested in predicting the lowest melting point achievable by any given pair. All temperature values presented here are in Kelvin unless otherwise stated.

After filtering duplicates, we take a stratified sample of mixtures (which we refer to as A,B pairs) and individual components (A,A pairs) into the training and test set (90% and 10%, respectively). We then divide the molten salt training set into 10 stratified folds for cross-validation.

### 3.5 Architecture

For each eutectic mixture pair, both molecules' graphs are passed through a set of identical AttentiveFP GNN layers; these combine a message passing GNN framework with an attention mechanism to account for intramolecular interactions beyond each node's one-hop neighborhood.<sup>20</sup> These layers output a feature embedding for each molecule (referred to as F(A) and F(B) in Fig. 6).

The interactions between the two molecules in the mixture influence its melting temperature, so rather than computing a similarity or difference metric between the two, we concatenate the two molecule representations so that the following layers can learn a function of the molecules' interactions. By concatenating A and B, it is possible for the fully connected layers in the Siamese branches to learn something about the interactions between the two molecules, as opposed to only learning their difference.

However, concatenating them implies an ordering, and because we are not incorporating information about individual melting temperatures or mixture proportions, we cannot enforce a meaningful ordering between the two. We address this by utilizing the central idea from Janossy pooling to enforce

order invariance by concatenating the representations in every possible ordering, *i.e.* (A, B) and (B, A). One might extend to higher-order mixtures by implementing a permutation-sampling approximation of Janossy pooling, selecting a value  $n$  as the maximum number of permutations to be sampled per mixture.

These concatenated molecule representations are passed through Siamese branches consisting of fully connected layers, with dropout layers in between. The output of these branches are mean-pooled to generate a final order-invariant representation of the mixture pair, which is then passed through the output layer to predict  $T_e$ . A diagram of the architecture is depicted in Fig. 6, and all selected hyperparameters and optimization methods are detailed in Table 3.

### 3.6 Transfer learning

Because we have much less organic data than we do inorganic data, rather than training a model from random initialization for our organic datasets, we use transfer learning to see if our learned molecule features from AttentiveFP in the inorganic model can be applied to eutectic melting point prediction for organic molecules. We extract features from the AttentiveFP layers for the organic DES molecules, perform principal

**Table 3** We used Bayesian Optimization with Hyperband (BOHB) for hyperparameter tuning in all our experiments. We used the Pytorch implementations of the Adam optimizer and LinearLR learning rate scheduler for all optimizers. Models were trained for up to 1000 epochs with early stopping after 100 epochs of no improvement

Hyperparameter	Selected value
Batch size	256
Learning rate	0.001
LR Scheduler start factor	0.350
LR Scheduler iterations	481
Embedding size	128
Hidden channels	256
AttentiveFP layers	6
AttentiveFP timesteps	4
Dropout 1	0.383
Fully connected layer 1 size	8
Dropout 2	0.002
Fully connected layer 2 size	8

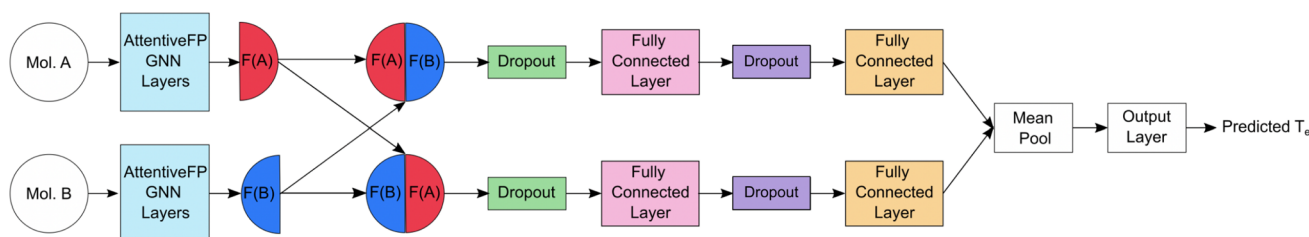


**Fig. 6** Our architecture begins with the graph structure for each molecule in the pair passing through an identical set of AttentiveFP GNN layers. The resulting feature embeddings of each molecule are concatenated in both possible orderings, based on the idea of Janossy pooling. Then both versions are passed through Siamese fully connected layers with dropouts. We compute the mean of the two branches to generate the mixture feature embedding, and then go through one more layer to get the predicted  $T_e$  value. This is an order-invariant architecture which can learn  $T_e$  prediction without relying on complex, engineered features.



component analysis (PCA) to reduce their dimensionality, and then train a kernel ridge regression (KRR) model for DES eutectics on this reduced set of features.

## 4 Experiments and results

First, we perform experiments training our architecture on binary molten salt eutectic mixtures and molten salt individual components. The eutectic datasets we use come from ref. 11, 13 and 15–17. Then we perform transfer learning experiments with organic eutectic datasets to see how well our model can extrapolate. We evaluate model performance in terms of root mean squared error (RMSE), mean absolute error (MAE), mean absolute percentage error (MAPE), and coefficient of determination ( $R^2$ ). The DES, fatty acids, explosives, and quinones datasets all consist of organic molecules, whereas our main dataset of molten salts is inorganic. All molecules' atom and bond structures, and melting points for the 149 molten salt individual components, are sourced from Pubchem.<sup>27</sup> The data from Lavrinenko *et al.*<sup>16</sup> also includes individual component melting points.

### 4.1 Molten salts experiments

The first experiment is to train a model on the molten salt eutectics. We use Bayesian Optimization with Hyperband (BOHB)<sup>29</sup> for hyperparameter tuning. This method combines two existing hyperparameter optimization methods, Bayesian optimization and Hyperband, in order to achieve strong performance, scalability, and effective use of parallel resources, where the two methods individually had significant trade-offs between these.

We train some models using only the molten salt eutectic mixtures, which we refer to as A,B pairs. We also train some models using both the molten salt eutectic mixtures and the individual components for which we have melting point values, in order to test whether augmenting the dataset with these individual components may improve model performance. The individual components are represented as pairs in which both components are identical, which we call A,A pairs. We compare the performance of models trained in these two ways (Fig. 7), and evaluate whether the individual component data is useful for data augmentation.

### 4.2 Molten salts results

Overall, our model is able to achieve a  $R^2$  of 0.93 in predicting eutectic melting temperatures for binary molten salt eutectics. Models trained with A,A pairs included in the training data perform better than those trained only on binary mixtures. Although the performance difference on the full test set is small, the difference appears much more significant when looking at the subset of data with  $T_e \leq 500$  K, where we achieve an RMSE of 59.53 K. We emphasize this subset because mixtures with low melting points are of greatest interest when screening eutectic materials. The training set only included 134 individual component data points, so it seems unlikely that this improvement in performance can be attributed entirely to the greater quantity of data. This suggests future experiments in using lower-order mixture data to augment training data on higher-order mixtures, and *vice versa*.

We emphasize that these single component melting points are used as data points, not features. When we compare these results to the exact same architecture and feature

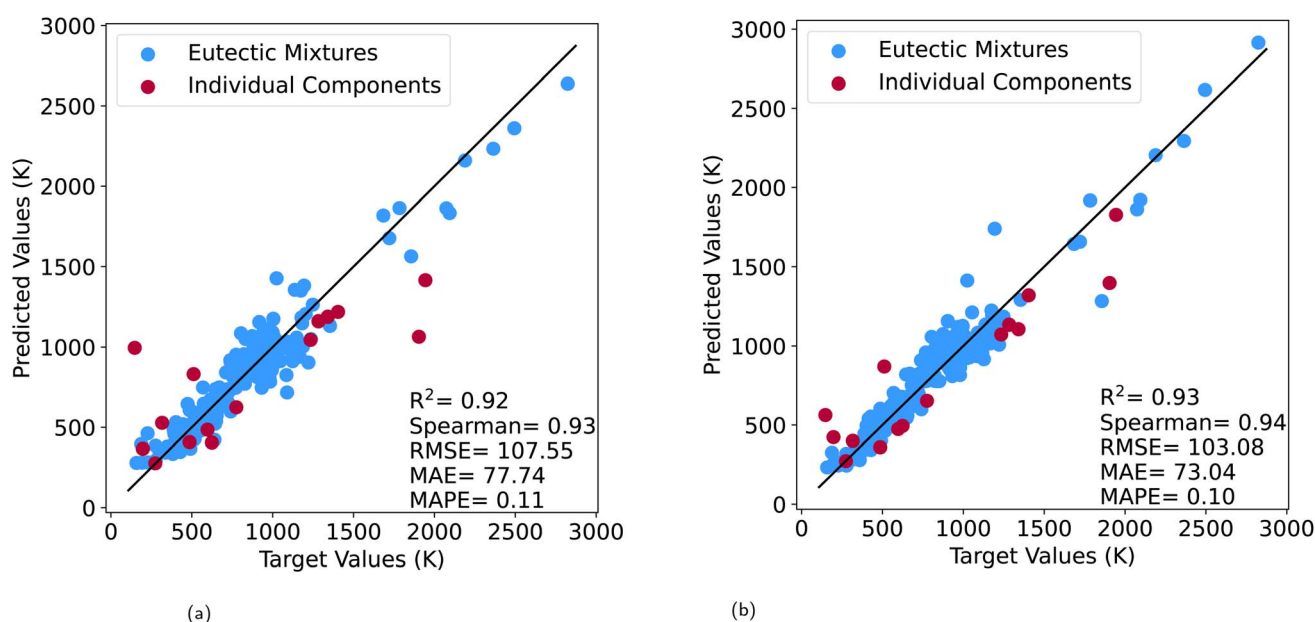


Fig. 7 Metrics on each plot correspond to the predictive performance on the A,B test set; they do not include the performance on individual components' melting points. The model which included A,A pairs in training has slightly lower test error overall, and achieves an RMSE of 59.53 K on mixtures below 500 K, more than 10° better than the model which only trained on A,B pairs. (a) Trained on mixtures only A,B. (b) Trained on mixtures and individual components (A,B and A,A).



**Table 4** Performance results. All error values in degrees K. Datasets marked with \* include mixtures of >2 components. Rows in bold text represent the best performance on the given dataset. The model trained on A,A and A,B data consistently outperforms the model trained only on A,B data. In some cases this is a very small difference, but in low temperatures (<500 K) there is a difference of 12.51 K between the two models' RMSE values. In addition, the A,A + A,B model is able to predict individual component melting points with all error metrics better than the trivial baseline, despite having only 134 individual components in the training data

Dataset	Model	RMSE	MAE	MAPE	$R^2$	Std. dev.	Baseline MAE	Baseline MAPE
Full dataset from ref. 1*	ITM	86.6	—	—	—	—	—	—
Test set from ref. 1*	Mean model	65.4	—	—	—	—	—	—
Random partition from ref. 1	A,B only, trained on <sup>1</sup>	95.45 ± 13.76	68.90 ± 10.29	0.09	0.92	309.86	220.23	0.85
A,B test set	A,A + A,B	<b>103.08 ± 20.05</b>	<b>73.04 ± 9.09</b>	<b>0.10</b>	<b>0.93</b>	369.9	267.5	0.46
A,B test set	A,B only	107.55 ± 11.79	77.74 ± 9.42	0.11	0.92	369.9	267.5	0.46
A,B where $T_c < 500$ K	A,A + A,B	<b>59.53 ± 10.33</b>	<b>47.73 ± 9.27</b>	<b>0.13</b>	<b>0.60</b>	78.41	63.11	0.19
A,B where $T_c < 500$ K	A,B only	72.04 ± 20.03	49.76 ± 15.03	0.15	0.48	78.41	63.11	0.19
A,A test set	A,A + A,B	<b>231.61 ± 86.17</b>	<b>189.56 ± 69.85</b>	<b>0.44</b>	<b>0.89</b>	629.34	443.35	0.81
A,A test set	A,B only	372.26 ± 169.92	275.45 ± 129.39	0.67	0.64	629.34	443.35	0.81

representation trained on A,B pairs only, we see that the gain in performance is approximately 4.5° on the overall set, and 12.5° in the low temperature subset. Table 4 shows that the model trained on A,A and A,B pairs have improved performance on all test sets compared to the model trained only on A,B pairs.

As shown in Fig. 8, our model trained on A,B and A,A pairs also achieves prediction on individual components' melting points with a  $R^2$  of 0.89, and a RMSE of 231.61 K. In the context of the standard deviation of the A,A dataset, this prediction error is one-third of the RMSE of a baseline trivial model (the best possible constant model), indicating that despite the relatively large numerical value of the RMSE, the model has learned significant predictive information. This suggests that by

including only small quantities of A,A data in training, the final model can learn to estimate individual component melting points while also achieving improved prediction performance on A,B mixtures.

A recent work by Ravichandran *et al.*<sup>1</sup> also used subsets of Janz *et al.*<sup>13</sup> to train machine learning models for eutectic melting temperature prediction; their selection of binary mixtures is a subset of those used in our work. While their experiments resulted in lower RMSE values than ours, their proposed methods require all individual component melting points and enthalpies (ITM method), manually curated engineered features (GBM method), or  $x_e$  values (Roost method), none of which are required by our method. For comparison, we took a random training and test partition of the binary mixtures used in their dataset, and trained our architecture on that partition using only structural information. The results, as shown in Table 4, indicate that our model can achieve performance close to the ITM without requiring individual component melting points and enthalpies.

We note that differences in performance may also be in part due to the difference in our datasets; they considered a narrower selection of binary mixtures than ours, and included other  $n$ -ary mixtures which we did not.

### 4.3 Deep eutectic solvents transfer learning experiments

We next examine the trained model's ability to extrapolate to organic mixtures. We use 88 individual components and 239 unique mixtures drawn from ref. 15–17, to partition into training and test sets for transfer learning experiments. These data sources included some fatty acids, however we excluded these from the dataset because we planned to test extrapolation to a different fatty acid dataset. The training set had 78 single components and 190 mixtures; the test set had 10 single components and 49 mixtures.

First, we select the molten salts model which performs best on our DES training set. Organic training data including both A,A and A,B pairs were input into our architecture, and then the molecule features output by the AttentiveFP layers (F(A) and

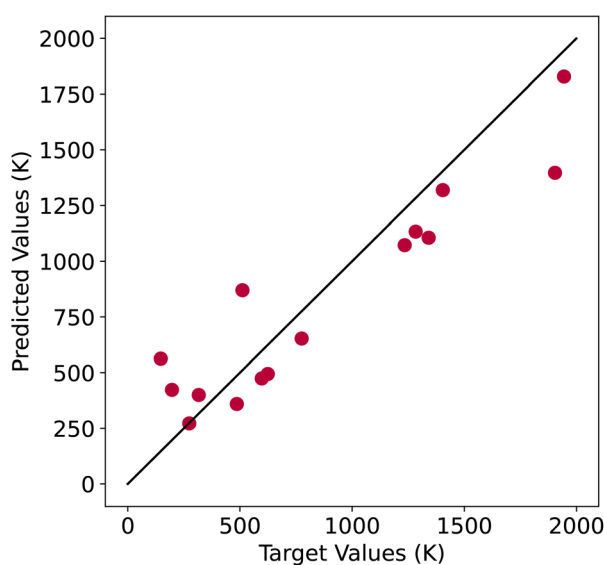


**Fig. 8** The model trained on A,A and A,B molten salts predicts on individual components with an  $R^2$  of 0.89 for the whole A,A test set. This model also performs better on binary eutectic mixtures than the model trained on A,B pairs only. This suggests that augmenting the binary mixture data with individual components' melting point data can improve model predictions on both individual and mixture materials.



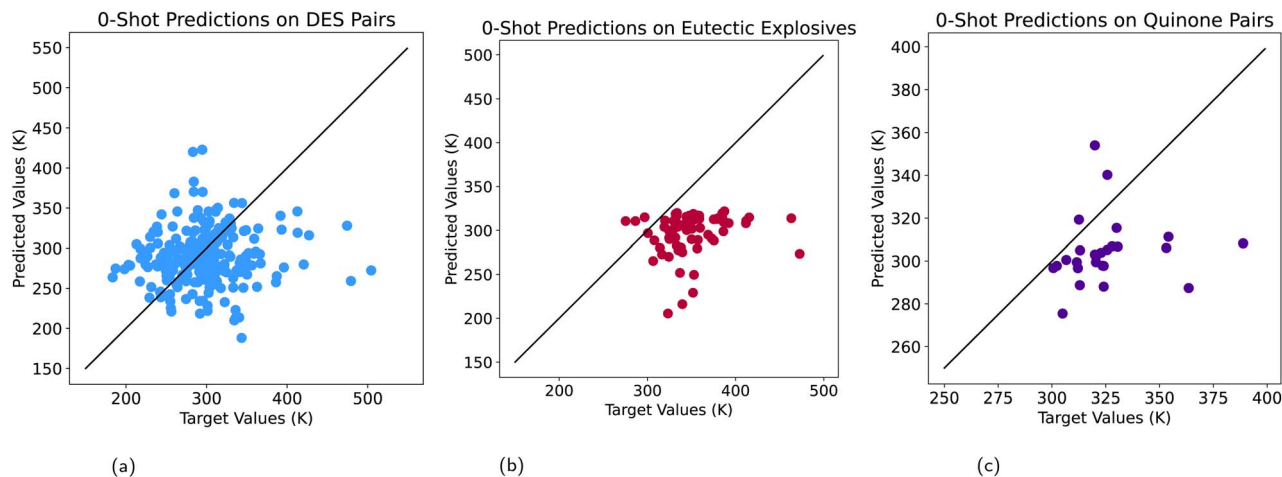


Fig. 9 The model trained on inorganic A,A and A,B molten salts assigns similar values to similar molecules, and groups organic mixtures in a reasonable temperature range. (a) Predictions on DES data. (b) Predictions on eutectic explosives. (c) Predictions on quinones.

F(B)) were extracted. We scale the features and then use (PCA) to reduce them from 256 features per molecule to 5 features per molecule. We then concatenate each molecule pair in both possible orders, and fit a kernel ridge regression model to the data. We use a grid search to determine the optimal kernel ridge regression hyperparameters. We evaluate the best model on the DES test set, as well as evaluate zero-shot predictions on other smaller organic datasets.

#### 4.4 Deep eutectic solvents results

The zero-shot predictions from the molten salt A,A + A,B model chosen for transfer learning on organic A,B pairs can be seen in Fig. 9–11.

Some models trained on molten salts are able to assign organic materials to the correct average melting temperatures of their corresponding molecule family (*e.g.* fatty acids) despite having never seen an organic molecule in training. These models are also able to assign families of closely-related molecules to similar values; for example, all quinone mixtures

receive similar predictions, and fatty acid mixtures' predictions form distinct patterns. This indicates that our model is learning similar feature embeddings for mixtures that we expect to be similar to one another. Therefore, the molecule representation learned by the GNN layers of our architecture from inorganic data can be used for transfer learning to organic DES data to achieve improved predictions on DES mixtures. However, our KRR model transfers less well to both the explosives and quinone datasets.

Mixtures from the same family of materials have predictions that are close together; fatty acids, in particular, seem to follow a distinct trend. This suggests that mixtures that belong to the same family are being assigned similar learned feature embeddings; these are the molecule graph features that we extract from our GNN layers. Then we scale, apply PCA, and fit the kernel ridge regression model.

Through this process, we are able to predict DES  $T_c$  values with an RMSE of 37.57 K. We are also able to predict melting

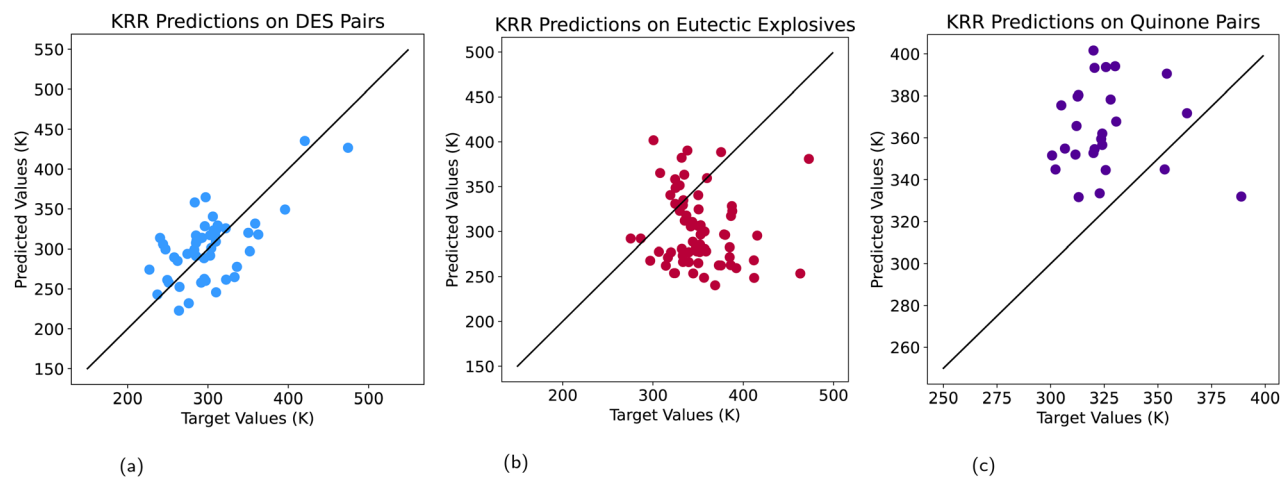
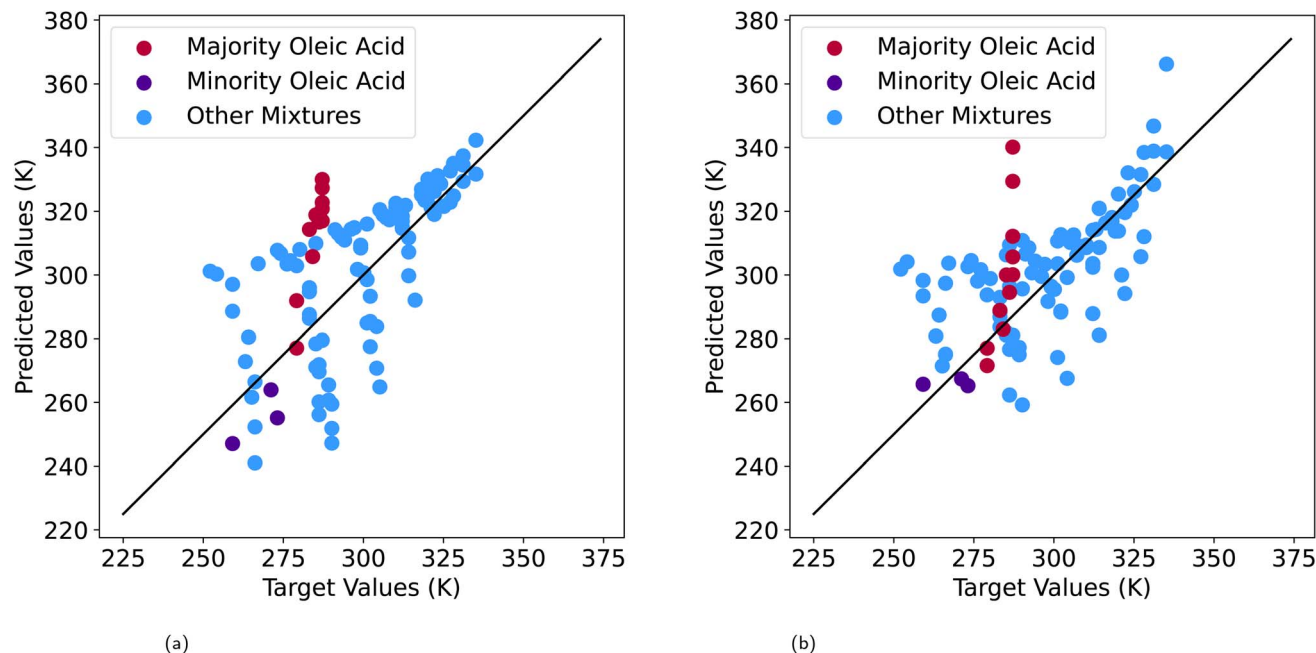


Fig. 10 After extracting DES features from the A,A + A,B model, fitting a kernel ridge regression model to a training DES subset, and testing on the remaining data, our DES test predictions have improved. However, this model performs poorly on explosives and quinones. (a) Predictions on DES data. (b) Predictions on eutectic explosives. (c) Predictions on quinones.





**Fig. 11** Prediction results on fatty acids. (a) presents 0-shot predictions from the model trained on molten salts, while (b) presents predictions after extracting DES features from the A,A + A,B model, fitting a kernel ridge regression model, and then testing on fatty acids. Models from our experiments frequently made predictions on fatty acid eutectic mixtures which had a strong linear correlation with the target values. Mixtures including oleic acid consistently “branched” off from the rest of the group. This data was computed using an ideal thermodynamic model by Kahwaji *et al.*<sup>11</sup> This suggests our architecture is able to learn a function correlated with the ideal thermodynamic model without having information about individual components’ melting points or enthalpies of melting. (a) Predictions from molten salts model. (b) Predictions from transfer learning KRR with DES.

temperatures of the individual components from the DES dataset with an RMSE of 67.30 K (Table 5).

The most relevant work for comparison is Odegova *et al.*,<sup>17</sup> from which we obtain the majority of our DES dataset. Their work

achieves an RMSE of 41 K, but requires much more expensive features than our work, including the individual component melting points and corresponding  $x_e$  values. However, their overall goal is to predict the melting points at any given mixture

**Table 5** Feature extraction and KRR results for organic data. All error values in degrees K. Rows in bold text represent the best performance on the given dataset

Dataset	RMSE	MAE	MAPE	$R^2$	Std. dev.	Baseline MAE	Baseline MAPE
<b>0-shot prediction from best molten salt model</b>							
DES test set	90.26 ± 16.20	71.64 ± 16.33	0.25	0.05	69.96	51.7	0.12
Fatty acids test set	43.97 ± 5.23	36.73 ± 5.02	0.12	0.29	20.15	17.25	0.06
Explosives <sup>12</sup>	63.19 ± 13.31	51.32 ± 10.31	0.14	0.04	35.32	25.73	0.07
Quinones <sup>28</sup>	75.31 ± 13.22	67.21 ± 13.34	0.21	0.33	19.62	12.95	0.04
<b>0-shot prediction from molten salt model chosen for transfer learning</b>							
DES test set	55.79 ± 13.25	40.58 ± 10.84	0.13	0.0	69.96	51.7	0.12
Fatty acids test set	20.73 ± 2.87	16.56 ± 2.45	0.06	0.38	20.15	17.25	0.06
Explosives <sup>12</sup>	<b>66.69 ± 12.41</b>	<b>56.37 ± 8.89</b>	<b>0.16</b>	<b>0.03</b>	35.32	25.73	0.07
Quinones <sup>28</sup>	<b>31.30 ± 10.02</b>	<b>24.97 ± 8.16</b>	<b>0.07</b>	<b>0.01</b>	19.62	12.95	0.04
<b>KRR transfer learning predictions</b>							
DES test set	37.57 ± 4.55	<b>31.21 ± 4.29</b>	<b>0.11</b>	<b>0.41</b>	69.96	51.7	0.12
DES AA test set	67.30 ± 24.77	47.17 ± 20.09	0.12	0.62	77.05	61.32	0.17
<b>0-shot prediction from KRR model</b>							
Fatty acids test set	<b>18.11 ± 2.64</b>	<b>13.34 ± 1.73</b>	<b>0.05</b>	<b>0.39</b>	20.15	17.25	0.06
Explosives <sup>12</sup>	75.53 ± 7.80	62.91 ± 7.47	0.17	0.02	35.32	25.73	0.07
Quinones <sup>28</sup>	48.60 ± 5.01	44.08 ± 5.36	0.14	0.0	19.62	12.95	0.04
<b>Other works for comparison</b>							
Odegova <i>et al.</i> <sup>17</sup>	41.00	—	—	0.78	77	—	—



ratio, which differs from our work which is trying to predict the minimum reachable eutectic melting point regardless of ratio.

#### 4.5 Testing on fatty acids and other organics

Our zero-shot prediction results on fatty acids across several models frequently have a strong linear correlation with the target values, and when plotted, appear to form two branches in which mixtures with and without oleic acid appear to follow two different linear slopes. Some fatty acid mixtures are themselves deep eutectic solvents, but these correlations also occur in models trained only on molten salts, before any DES transfer learning. We are not aware of any fundamental chemical relationship between molten salts and fatty acids that would explain this.

The KRR model trained on DES data has slightly better zero-shot performance on fatty acids than zero-shot predictions directly from the molten salts model. The molten salt A,A + A,B model zero-shot predictions for fatty acids follow a trend roughly aligned with the  $x = y$  line with performance approximately equal to trivial baselines, while after transfer learning and KRR, all error values are slightly better than the trivial baselines. This result is meaningful: achieving baseline-level zero-shot performance indicates that the trained model correctly identifies the approximate average eutectic melting temperature of fatty acids, which exhibits a standard deviation of only about 20 K across the test set. Given that the molten salt training data have a standard deviation roughly an order of magnitude larger, this represents a significant achievement.

Both the zero-shot predictions from the molten salts model and the KRR model that was trained with deep eutectic solvent data are able to perform well on the fatty acids. The fatty acids are the only computationally generated dataset we examined in this work, as Kahwaji *et al.*<sup>11</sup> used the ideal thermodynamic model to compute these. Furthermore, fatty acids are themselves a type of deep eutectic solvent, although we ensured that the fatty acids in this set were not present in the DES training or test sets. Both of these factors could potentially make this set an easier extrapolation problem than the explosives or quinone sets.

We also include test results on explosive eutectics<sup>12</sup> and quinones.<sup>28</sup> Our predictive performance on these datasets is poor in the context of their respective baselines. However, the neural network and KRR predictions are informative with regards to our models' ability to recognize which mixtures belong to similar families.

## 5 Discussion

### 5.1 Learning $T_e$ without engineered features

Our architecture is the only method we are aware of that uses only structural information to predict mixture  $T_e$  values. Although methods which require individual components' melting points, enthalpy values, or  $x_e$  values may achieve lower prediction error than our method, those same requirements present serious barriers to actually using those methods for high-throughput screening. In contrast, element composition and graph structure as described in Fig. 3 are easily accessible for any known molecule.

### 5.2 Data augmentation with single components

Our experiments which include A,A pairs in training data suggest that we can augment binary mixture data with individual component data to improve performance. Doing so also enables us to use the same trained model to make melting point predictions for new individual components; here we demonstrate performance significantly better than the trivial baselines in all metrics that we evaluated. This also suggests future work in which we augment  $n$ -ary mixture data with any lower-order mixture data.

### 5.3 Transfer learning and extrapolation

Typically when training on inorganic materials and testing on organic materials, we expect to see overprediction of melting temperatures. This is because materials with more ionic bonds tend to have higher melting temperatures; as a result, models trained on inorganic materials, where ionic bonds are very common, often learn to map all inputs to higher values than they would if they had been trained on organic materials. However, the model selected for transfer learning did not display this overpredicting behavior. This is a desirable property in a model to be used for transfer learning, since the organic mixtures' predicted melting points are already close to the correct values.

Feature extraction and KRR, using DES training data, results in improved predictions on the DES test set, as expected. However, this model still appears unable to extrapolate to other families of organic mixtures, such as explosives and quinones. The same model performs well on fatty acids, which are a type of deep eutectic solvent not seen during model training. Therefore it is possible that the difficulty of extrapolating to explosives and quinones is because these families of materials are not similar enough to deep eutectic solvents.

Our results on the computationally-generated fatty acids dataset suggest that our model is learning a function correlated with the ideal thermodynamic model despite not requiring any individual component melting point or enthalpy data.

## 6 Conclusions

In this work, we develop a GNN that learns an order-invariant model of melting points for binary eutectic mixtures using minimal data. By using Siamese neural network branches to compute both possible orderings of concatenated molecule representations, we are able to leverage information about the interactions between the two molecules in predicting the melting point of the mixtures.

Our architecture is able to learn eutectic melting points from only the graph structure and element composition of the molecules in the mixture, and to learn models that are correlated with the ideal thermodynamic model without requiring the  $x_e$  value, individual components' melting points, or enthalpies. As a result, this architecture can be used to screen a much wider variety of materials than comparable methods, drastically reducing the barriers to high-throughput screening for eutectic mixtures. This has the potential to speed up



materials design for sustainable energy applications such as development of battery electrolytes, thermal energy storage materials, and molten salt nuclear reactors.

This method is also able to use individual components' melting temperature data to augment the eutectic mixture data, leading to both improvements in the prediction of melting temperatures for mixtures, as well as the ability to predict additional individual components' melting temperatures.

We also publish a curated dataset of 2244 molten salt eutectic pairs, including their structural information and eutectic melting points, in order to promote further research by the community.

## Conflicts of interest

There are no conflicts to declare.

## Data availability

All data, data sources, and code repository are available at DOI: <https://doi.org/10.5281/zenodo.5483596>.

Code repository is also available at: [https://github.com/nilamandal/SGNN\\_Eutectic\\_Mixtures/](https://github.com/nilamandal/SGNN_Eutectic_Mixtures/).

## Acknowledgements

This work was supported by the NASA CT Space Grant and the National Science Foundation under Grant No. DMR-2102406. We thank Dr Antonio Baclig for helpful insights and discussion during this project.

## Notes and references

- 1 A. Ravichandran, S. Honrao, S. Xie, E. Fonseca and J. W. Lawson, *J. Phys. Chem. Lett.*, 2024, **15**, 121–126.
- 2 P. Bhatnagar, S. Siddiqui, I. Sreedhar and R. Parameshwaran, *Int. J. Energy Res.*, 2022, **46**, 17755–17785.
- 3 Y. Wang, C. Zhu, M. Zhang and W. Zhou, *Nuclear Power Reactor Designs*, Elsevier Inc, 2024, pp. 163–183.
- 4 D. Chicco, in *Siamese Neural Networks: An Overview*, ed. H. Cartwright, Springer US, New York, NY, 2021, pp. 73–94.
- 5 R. L. Murphy, B. Srinivasan, V. A. Rao and B. Ribeiro, *Janossy Pooling: Learning Deep Permutation-Invariant Functions for Variable-Size Inputs*, ICLR, 2019.
- 6 Y. Zhang and E. J. Maginn, *J. Chem. Phys.*, 2012, **136**, 144116.
- 7 V. Venkatraman, S. Evjen, H. K. Knuutila, A. Fiksdahl and B. K. Alsberg, *J. Mol. Liq.*, 2018, **264**, 318–326.
- 8 G. Sivaraman, N. E. Jackson, B. Sanchez-Lengeling, Á. Vázquez-Mayagoitia, A. Aspuru-Guzik, V. Vishwanath and J. J. De Pablo, *Mach. Learn.: Sci. Technol.*, 2020, **1**, 025015.
- 9 K. Low, R. Kobayashi and E. I. Izgorodina, *J. Chem. Phys.*, 2020, **153**, 1–13.
- 10 Z. Acar, P. Nguyen and K. C. Lau, *Appl. Sci.*, 2022, **12**, 2408.
- 11 S. Kahwaji and M. A. White, *Thermochim. Acta*, 2018, **660**, 94–100.
- 12 R. D. Chapman and J. W. Fronabarger, *Propellants, Explos., Pyrotech.*, 1998, **23**, 50–55.
- 13 G. J. Janz, C. B. Allen, J. R. Downey and R. P. Tomkins, *National Standard Reference Data Series*, 1978, pp. 1–243.
- 14 A. Guendouzi and S. M. Mekelleche, *Chem. Phys. Lipids*, 2012, **165**, 1–6.
- 15 R. K. Luu, M. Wysokowski and M. Buehler, *Appl. Phys. Lett.*, 2023, **122**, 234103.
- 16 A. K. Lavrinenko, I. Y. Chernyshov and E. A. Pidko, *ACS Sustain. Chem. Eng.*, 2023, **11**, 15492–15502.
- 17 V. Odegova, A. Lavrinenko, T. Rakhmanov, G. Sysuev, A. Dmitrenko and V. Vinogradov, *Green Chem.*, 2024, **26**, 3958–3967.
- 18 J. Gilmer, S. S. Schoenholz, P. F. Riley, O. Vinyals and G. E. Dahl, *International Conference on Machine Learning*, 2017.
- 19 W. L. Hamilton, *Graph Representation Learning*, 1st edn, Springer Cham Cham, 2020.
- 20 Z. Xiong, D. Wang, X. Liu, F. Zhong, X. Wan, X. Li, Z. Li, X. Luo, K. Chen, H. Jiang and M. Zheng, *J. Med. Chem.*, 2020, **63**(16), 8749–8760.
- 21 K. Xu, W. Hu, J. Leskovec and S. Jegelka, *How Powerful Are Graph Neural Networks?*, ICLR, 2019.
- 22 M. Jeon, D. Park, J. Lee, H. Jeon, M. Ko, S. Kim, Y. Choi, A.-C. Tan and J. Kang, *Bioinformatics*, 2019, **35**, 5249–5256.
- 23 H. Altae-Tran, B. Ramsundar, A. S. Pappu and V. Pande, *ACS Cent. Sci.*, 2017, **3**, 283–293.
- 24 L. Torres, N. Monteiro, J. Oliveira, J. Arrais and B. Ribeiro, *2020 IEEE 20th International Conference on Bioinformatics and Bioengineering (BIBE)*, 2020, pp. 168–175.
- 25 C. Fotis, N. Meimmetis, A. Sardis and L. G. Alexopoulos, *Mol. Omics*, 2021, **17**, 108–120.
- 26 L. Ward, A. Agrawal, A. Choudhary and C. Wolverton, *npj Comput. Mater.*, 2016, **2**, 16028.
- 27 S. Kim, J. Chen, T. Cheng, A. Gindulyte, J. He, S. He, Q. Li, B. A. Shoemaker, P. A. Thiessen, B. Yu, L. Zaslavsky, J. Zhang and E. E. Bolton, *Nucleic Acids Res.*, 2022, **51**, D1373–D1380.
- 28 E. Penn, A. Baclig, D. Ganapathi and W. C. Chueh, *Chem. Mater.*, 2023, **35**, 5255–5266.
- 29 S. Falkner, A. Klein and F. Hutter, *Proceedings of the 35th International Conference on Machine Learning, ICML 2018, Stockholm, Sweden, 2018*, pp. 1436–1445.

